Supplementary Information and Figures

SI 1) Evaluation of apoptotic-cell fragments.

Floating dead cell fragments were collected from apoptotic m-cardiomyocytes by centrifugation after treatment with etoposide. These fragments generated no adherent living cells after they were re-plated to a culture dish for up to 7 days, indicating that the samples contained no living cells. Soon after collection, 99.5±0.2% of the fragments were positive for propidium iodide (PI) staining, an indicator of dead cells. Therefore, contamination by live cells was unlikely when the floating cells were collected 24 h after etoposide treatment.

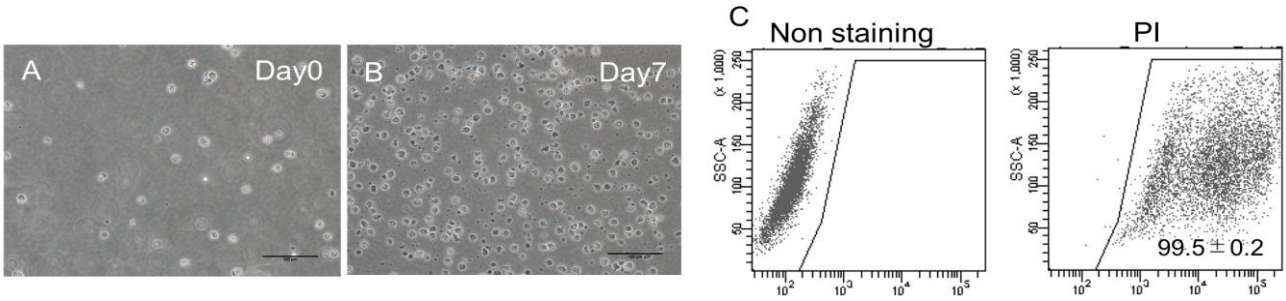

Figure S1. Apoptotic-cell fragments of m-cardiomyocytes. (A) m-cardiomyocytes treated with 50 μM etoposide for 24 h. Floating dead cell fragments were collected and plated on a culture dish. The picture was taken soon after plating. (B) No adherent live cells were observed 7 days after plating the cell fragments. Bars = 100 μm. (C) PI staining of apoptotic-cell fragments derived from m-cardiomyocytes.

SI 2) Controls for immunocytochemistry.

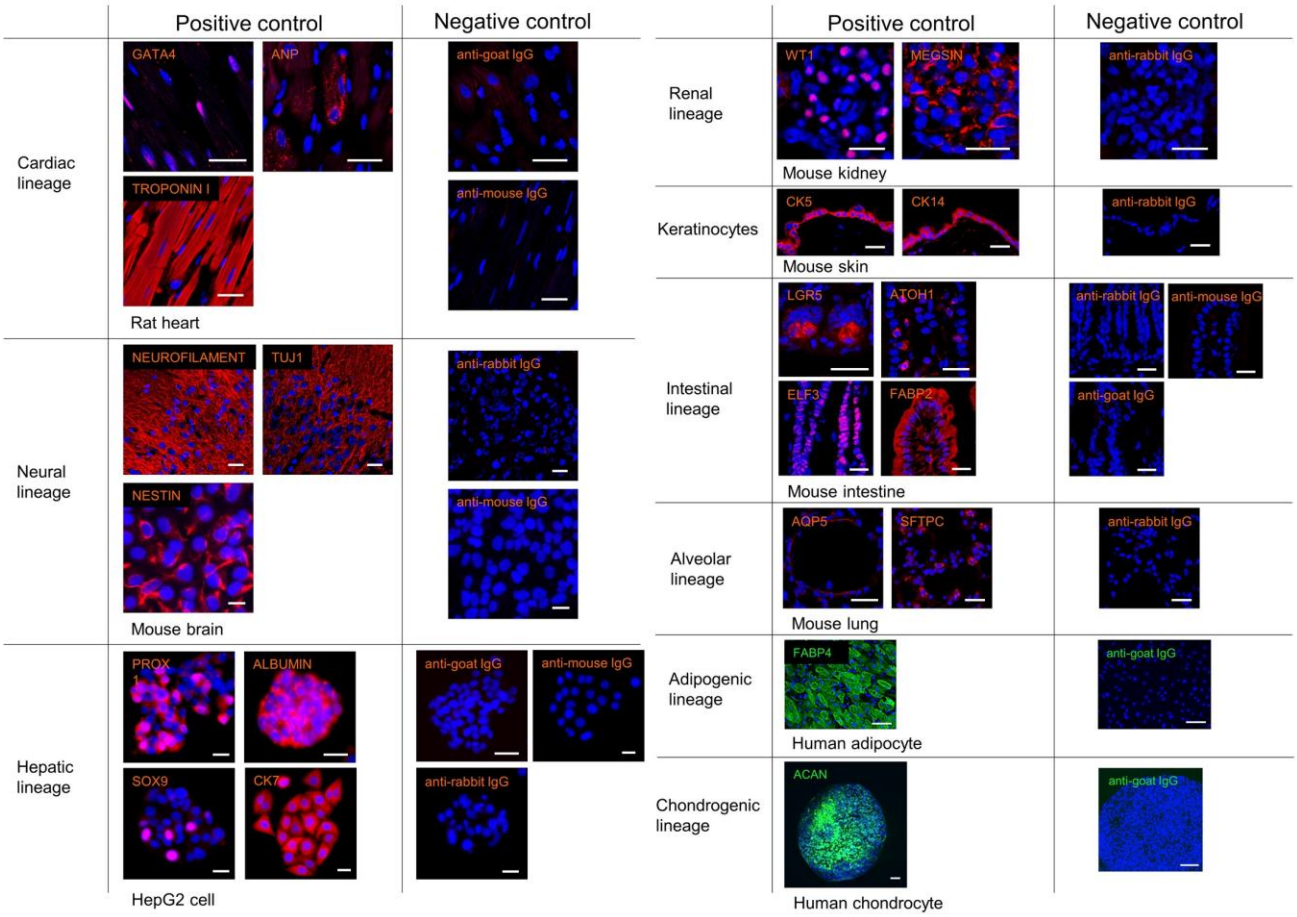

Figure S2A. Positive and negative controls for each immunocytochemical marker. Bars = 50 μm.

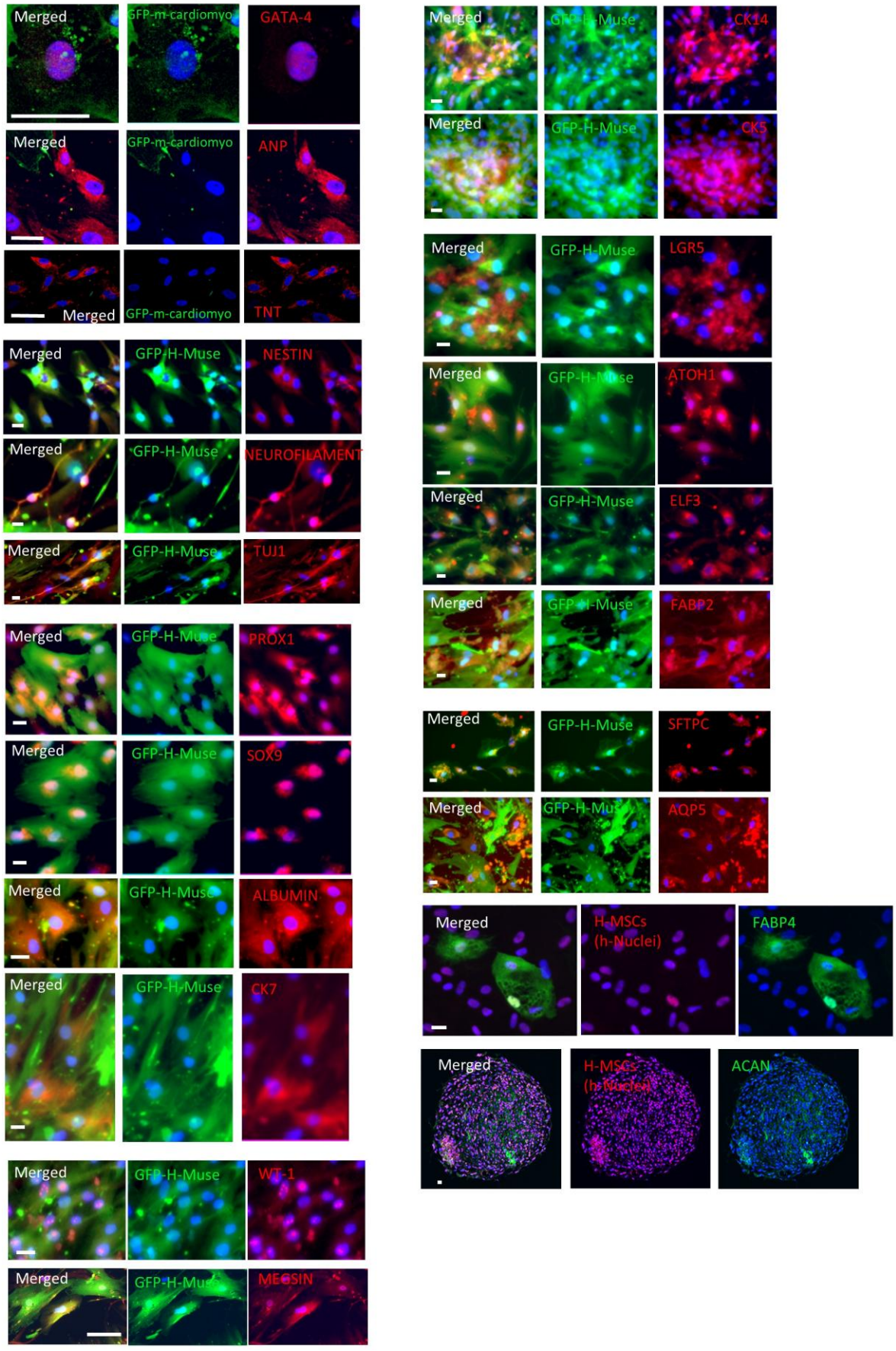

Figure S2B. Color codes for the immunocytochemical images. Bars = 25 μm.

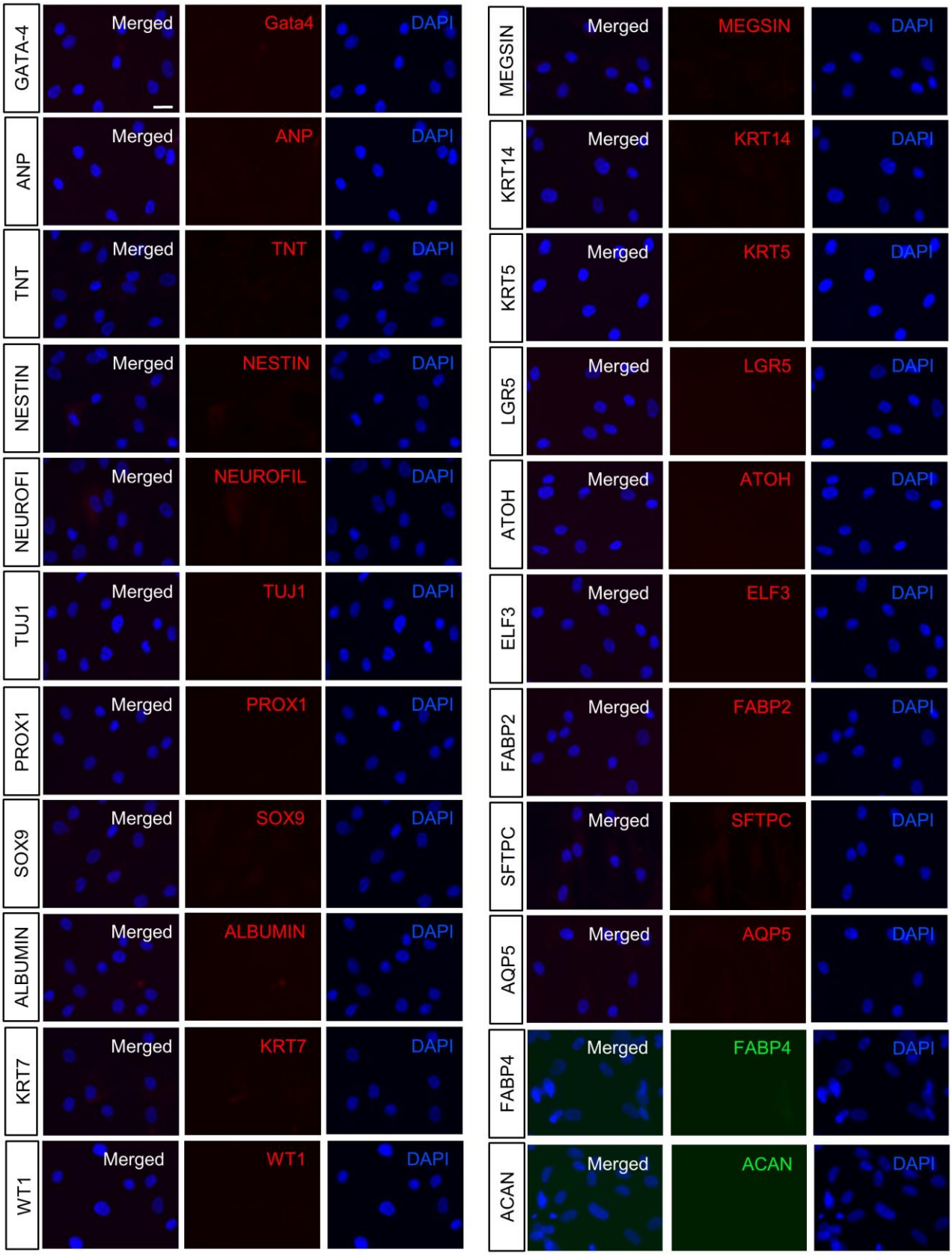

Figure S2C. Immunocytochemistry of naïve Muse cells.
None of the differentiation markers examined were expressed in naïve Muse cells. Bar = 50 μm.

SI 3) Differentiation marker expression in h-Muse cells after incubating with rat apoptotic fragments.

Rat differentiated cells were selected from mesodermal-, ectodermal-, and endodermal-lineages and apoptotic fragments were supplied to h-Muse cells for the first 3 days and then washed out. The h-Muse cells were transduced with GFP-lentivirus for identification in immunocytochemistry. Confirmed species-specific primers were used for the qPCR.

Co-culture with apoptotic renal cell fragments induced the expression of the human-specific progenitor markers *WT-1* and -*EYA1* at D3 ($p<0.001$) in h-Muse cells. The maturity marker human-aquaporin-1 (*AQP1*) was faintly expressed at D3 and upregulated at D14 and D21 ($p<0.001$; Fig. S3A). Ectodermal (human-*KRT10*, -*NEUN*) and endodermal (human-*PDPN*, -*AFP*) markers were consistently not detected by qPCR up to D21. Immunocytochemistry revealed expression of WT-1 at D14 and MEGSIN at D21 in h-Muse cells (Fig. S3B).

Keratinocyte fragments induced the expression of the stem cell markers human-p63 (*P63)* and -keratin15 (*KRT15*) at D3 ($p<0.001$), and the keratinocyte marker human desmoglein-3 (*DSG3*) at D5 ($p<0.001$). Another keratinocyte marker, human-*KRT10,* was faintly expressed at D3, upregulated at D14, and maximum at D21 ($p<0.001$; Fig. S3C). Mesodermal (human-*NKX2.5*, -*ANP*, -*TNT*) and endodermal (human-*PROX1*, -*LGR5*, -*PDPN*) markers were consistently under the detection limit in h-Muse cells in qPCR. Two keratinocyte markers, cytokeratin-14 (KRT14) and cytokeratin-5 (KRT5), were expressed at D21 in h-Muse cells (Fig. S3D).

Intestinal cell fragments induced human-*LGR5* (stem cell), -*ATOH1* (secretory progenitor), and -*GFI1* (goblet and Paneth cell progenitors) at D3 ($p<0.001$); and –*LYZ1* (Paneth cell) and -*FABP2* (enterocyte) at D8 ($p<0.001$) in h-Muse cells (Fig. S3E). Mesodermal (human-*NKX2.5*, -*ANP*, -*TNT*) and ectodermal (human-*KRT10*, -*NEUN*) markers were consistently under the detection limit in qPCR. LGR5 and ATOH1 were detectable in h-Muse cells at D5, ELF3 (enterocyte progenitor) at D14, and FABP2 at D21 by immunocytochemistry (Fig. S3F).

Alveolar cell fragments induced human-*PDPN* (progenitor/type 1 alveolar cell), aquaporin-5 (*AQP5*; type 1 alveolar cell), sodium channel epithelial 1α subunit (*SCNN1A*; lung epithelial), and *CDH1* (lung epithelial) at D3 ($p<0.001$), and these markers were upregulated over time (Fig. S3G). Mesodermal (human-*NKX2.5*, -*ANP*, -*TNT*) and ectodermal (human-*KRT10*, -*NEUN*) markers were consistently under the detection limit in qPCR. Surfactant protein-C (SFTPC; progenitor/ type 2 alveolar cell) was expressed at D7 and AQP5 at D14 in immunocytochemistry in h-Muse cells (Fig. S3H).

The percentage of each lineage-specific marker in h-Muse cells is summarized in Fig. S3I. Positive and negative controls for each marker in immunocytochemistry (Fig. S2A) and the color codes for immunocytochemistry (Fig. S2B) are shown in Fig. S2. Immunocytochemistry confirmed that expression of the differentiation markers was negative in naïve Muse cells (Fig. S2C).

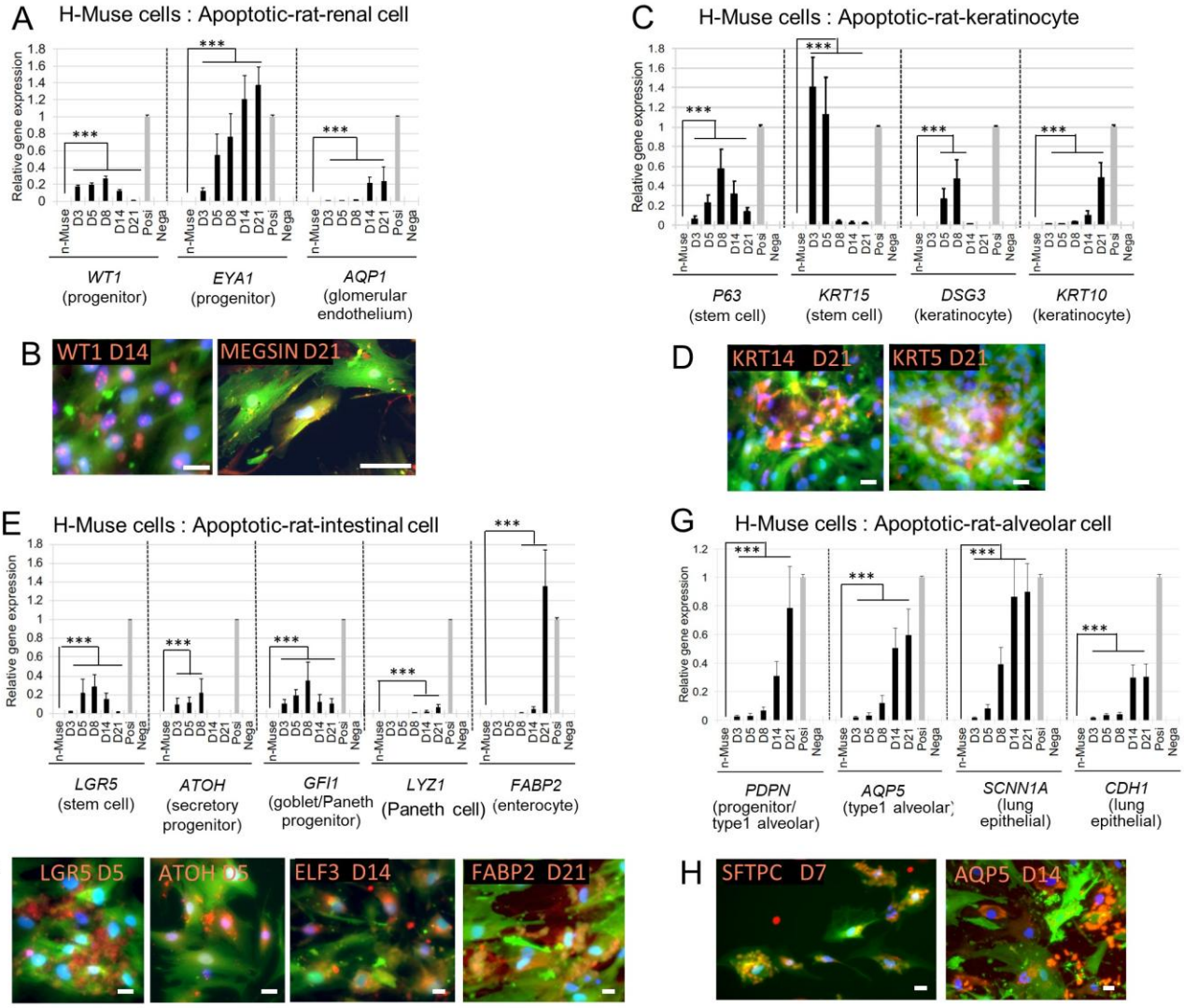

I

DDC cell type	markers expressed in h-Muse cells	% in h-Muse cells	day after incubation
Cardiomyocyte	GATA-4 (progenitor)	46.5±5.8%	D3
	ANP (cardiomyocyte)	52.6±5.7%	D14
	TNT (cardiomyocyte)	44.5±7.7%	D21
neural cell	NESTIN (neural stem/progenitor)	62.2±2.5%	D5
	NEUROFILAMENT M (mature neuronal cell)	41.0±1.7%	D21
	TUJ1 (mature neuronal cell)	39.6±5.7%	D21
Hepatic cell	PROX1 (liver progenitor)	46.3±2.1%	D5
	SOX9 (liver progenitor)	43.3±3.6%	D5
	ALBUMIN (hepatocyte)	22.2±4.4%	D21
	cytokeratin-7 (KRT7; cholangiocyte)	11.5±3.0%	D21
renal cell	WT-1 (renal progenitor marker)	31.7±5.6%	D14
	MEGSIN (mesangial cell)	13.9±3.1%	D21
Intestinal cell	LGR5 (Intestinal stem cell)	45.0±3.7%	D5
	ATOH1 (secretory progenitor)	35.7±4.3%	D5
	ELF3 (enterocyte progenitor)	38.4±3.0%	D14
	FABP2 (enterocyte)	21.1±3.4%	D21
Keratinocyte	cytokeratin-14 (KRT14; Keratinocyte)	41.3±3.6%	D21
	cytokeratin-5 (KRT5; Keratinocyte)	39.2±1.7%	D21
Alveolar cell	Surfactant protein-C (SFTPC; progenitor/ type 2 alveolar cell)	42.7±1.9%	D7
	aquaporin-5 (AQP5; type 1 alveolar cell)	25.4±3.2%	D14

Figure S3. Differentiation marker expression in h-Muse cells after incubating with rat apoptotic fragments. (A, C, E, G) Lineage-specific marker expression in qPCR and (B, D, F, H) immunocytochemistry in h-Muse cells after incubation with rat apoptotic cells. In qPCR, naïve h-Muse cells (n-Muse) and apoptotic cell fragments (Nega) were used as negative controls. ***: p<0.001. For the positive control, human fetus total RNA was used for renal cells, and keratinocytes; human small intestine RNA was used for intestinal cells; and human fetal lung RNA was used for alveolar cells. Graphs are represented as mean ± SEM. Bars; B, D, F, H = 25 μm. (I) Percent of marker expression in GFP-h-Muse cells after incubation with rat apoptotic cell fragments.

SI 4) Cardiac marker expression in h-Muse cells after incubation with apoptotic m-HL-1-fragments.

To evaluate the differentiation of h-Muse cells in quantitative reverse transcription-PCR (qPCR) assays, confirmed species-specific primers were used. When h-Muse cells were incubated with cell fragments derived from apoptotic m-cardiac muscle cell line (m-HL-1)-fragments at a 1:2 ratio for 3 days and then the fragments were washed out, the h-Muse cells became positive for human-*NKX2.5* and -*GATA-4* at D3 after starting the incubation and the positivity was maintained at D21. The h-Muse cells became positive for human atrial natriuretic peptide (*ANP*) at D7 and for human troponin-T (*TNT*) at D14. Ectodermal (human-cytokeratin10 [*KRT10*], -*NEUN*) and endodermal (human-*PROX1*, -*LGR5*, -*PDPN*) markers were consistently under the detection limit.

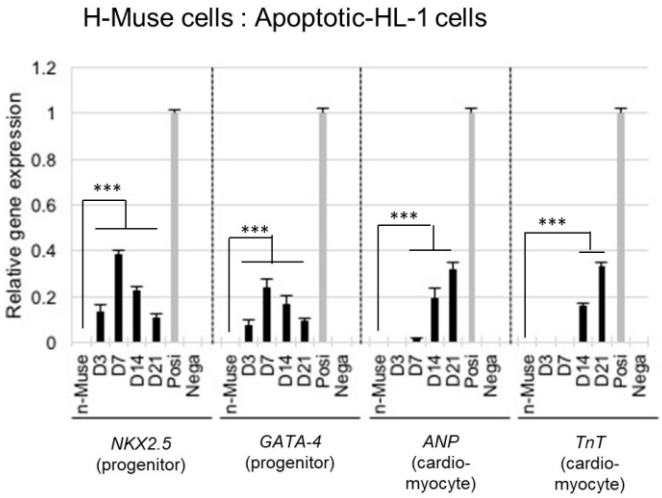

Figure S4. Cardiac marker expression in h-Muse cells after incubation with apoptotic m-HL-1 fragments. qPCR of human-specific *NKX2.5, GATA-4*, *ANP*, and *TNT* in h-Muse cells after incubation with apoptotic m-HL-1 fragments. Naïve h-Muse cells (n-Muse) and apoptotic cell fragments (Nega) were used as negative controls, and human fetal heart total RNA was used as a positive control (Posi). ***: p<0.001

SI 5) Evaluation of fusion by FISH analysis.

Cultures of the apoptotic mouse liver cell line Hepa1-6 (m-Hepa1-6) comprised dead cell fragments. Even so, it is considered that these cells might be revived by interacting with h-Muse cells during incubation. If they were revived, expression of the above-mentioned differentiation markers might be explained by the fusion of dead m-Hepa1-6 fragments and h-Muse cells. Therefore, to test the propensity of Muse cells to fuse with dead cells, intact m-Hepa1-6 and h-Muse cells were co-cultured at a 1:1 ratio

and fluorescence in situ hybridization (FISH) was performed. While over 4500 cells were analyzed, no fused cells were detected. Similarly, fusion between apoptotic m-Hepa1-6 fragments and h-Muse cells incubated at a 1:2 ratio for 3 days was not detected. Thus, fusion does not appear to be a major mechanism of h-Muse cell differentiation.

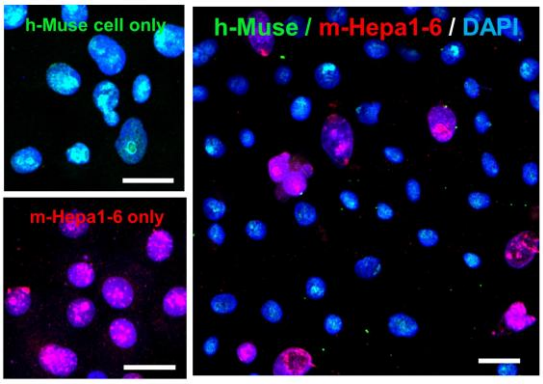

Figure S5. FISH analysis. Co-culture of h-Muse cells and intact m-Hepa1-6 at a 1:1 ratio for 3 days. Human nuclei are labeled green and mouse nuclei are labeled red. At 3 days, fusion between h-Muse cells and m-Hepa1-6 could not be detected, even after counting ~4500 cells. Incubation of h-Muse cells with apoptotic-m-Hepa1-6-fragments at a 1:2 ratio for 3 days showed the same tendency. Bars = 50 μm.

SI 6) Effect of conditioned medium, cell extract, and extracellular vesicles from apoptotic cells.

Apoptotic cells were prepared from m-cardiomyocytes and m-HL-1 cells.

Conditioned medium: One possible explanation for our observations is that humoral factors initiated the commitment of Muse cells to a specific-cell lineage. To test this possibility, we collected conditioned media from intact and apoptotic m-cardiomyocyte cultures at numbers that were 2x, 10x, or 100x higher than that of the h-Muse cells. These 6 kinds of conditioned media were centrifuged at low speed and passed through a 0.45-μm filter to remove intact cells and cell fragments. The h-Muse cells were then incubated with the conditioned medium, and qPCR was performed at 3, 7, 14, and 21 days. The conditioned media contained factors relevant to cardiac differentiation [1]; e.g., the conditioned medium from the culture containing 100x more apoptotic m-cardiomyocytes than Muse cells contained hepatocyte growth factor (HGF), cardiotrophin-1, and transforming growth factor beta 1 (TGF-β1; Fig. S6A). Human-specific cardiac markers, however, were consistently under the detection limit in h-Muse cells treated with any of the 6 kinds of conditioned media at any time-point. The same experiment was repeated using m-Hepa1-6 and mouse skeletal muscle cell line C2C12 (m-C2C12). Human-specific *PROX1*, α-fetoprotein (*AFP*), or albumin for incubation with m-Hepa1-6 conditioned media, and human-specific *PAX7*, *MYOD*, and *MYOGENIN* for m-C2C12 were under the detection limit for all conditions and time-points examined.

Cell extract: To test the possible involvement of cell extracts in Muse cell differentiation, intact m-cardiomyocyte cell extract was prepared by sonication. To avoid contamination by living cells in the apoptotic cell extracts, only floating dead cell fragments were collected after etoposide treatment, centrifuged, and subjected to sonication. Six cell extracts of intact and apoptotic m-cardiomyocyte

fragments from cultures containing a 2x, 10x, and 100x or greater number of m-cardiomyocytes than h-Muse cells were prepared and incubated with h-Muse cells. The cell extract containing 100x or more apoptotic m-cardiomyocyte fragments than Muse cells contained HGF, cardiotrophin-1, and TGF-1 (Fig. S6A). Human-specific cardiac markers, however, were under the detection limit in all conditions examined and at all time-points from 3 to 21 days. The same result was obtained with m-Hepa1-6 and m-C2C12 cells.

Extracellular vesicles: Another possible explanation for the h-Muse cell differentiation is that secreted extracellular vesicles containing cargo initiated the differentiation. To test this possibility, extracellular vesicles positive for CD63, TSG101, and HSP70 were collected by ultracentrifugation of medium from intact and apoptotic m-HL-1 cells (Fig. S6B, S6C). Extracellular vesicles contain microRNAs that regulate lineage specification [2]. Intact and apoptotic m-HL-1-derived extracellular vesicles contained miR-1, miR-133a, miR206, miR208, and miR-499, which are related to cardiac differentiation (Fig. S6D). Although the amount of extracellular vesicles required for differentiation induction differed among cell types in previous reports, most cases fall into the range of 25~100 μg/ml [3]. Therefore, we supplied 50 μg/ml and 200 μg/ml extracellular vesicles derived from intact and apoptotic m-HL-1 cells to h-Muse cells. Human-specific markers *NKX2.5*, *GATA-4*, *ANP*, and *TNT*, however, were under the detection limit in all conditions examined and at all time-points from 3 to 21 days. The uptake of extracellular vesicles into h-Muse cells was confirmed by incubating the h-Muse cells with PKH67-labeled extracellular vesicles for 3 days (Fig. S6E).

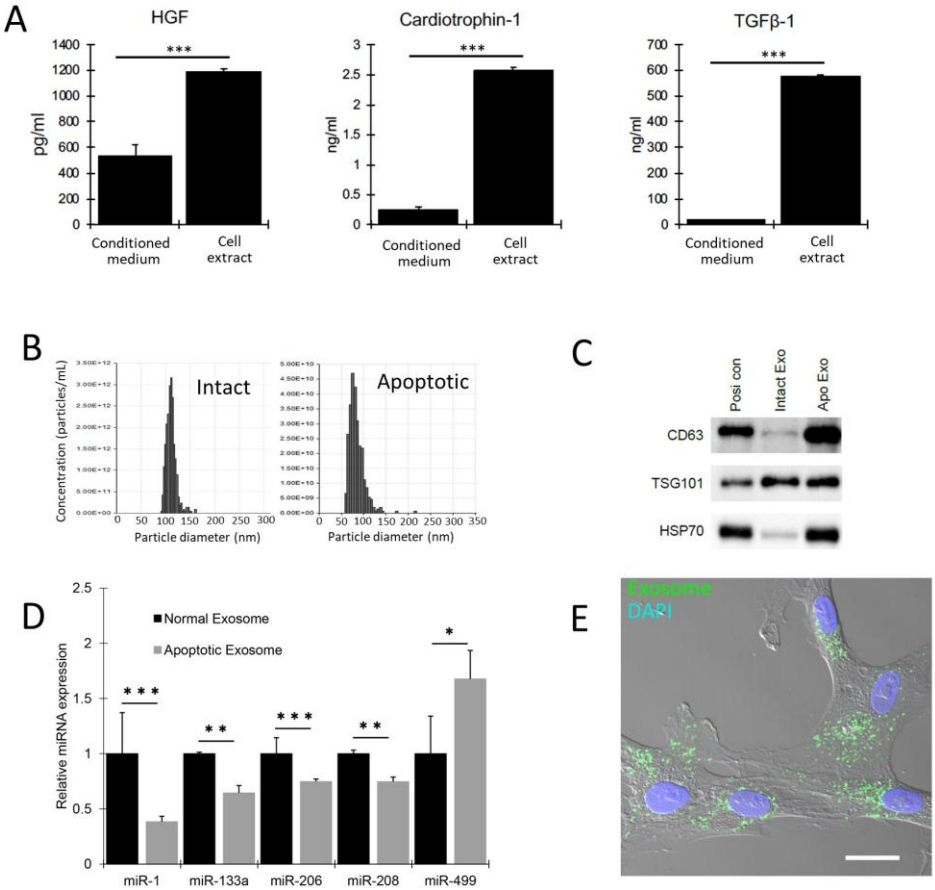

Figure S6. Conditioned medium, cell extract, and extracellular vesicles from apoptotic-m-cardiomyocytes had limited effects on cardiac marker expression in h-Muse cells. (A) ELISA for HGF, cardiotrophin-1, and TGF-β1 in apoptotic-m-cardiomyocyte-derived conditioned medium and cell extract. According to a previous report, 20 ng/ml HGF, 200 ng/ml cardiotrophin-1, and 2.5 ng/ml TGF-β were used for in vitro cardiac differentiation of Muse cells (Amin, et al., 2018). The amount of TGF-β1 was higher while the amounts of HGF and cardiotrophin-1 were lower in the conditioned medium and cell extract compared with the medium used for in vitro differentiation. ***; $p<0.001$. (B-E) Collection of extracellular vesicles from m-cardiomyocytes. (B) Tunable resistive pulse sensing analysis of extracellular vesicles derived from intact- and apoptotic-m-cardiomyocytes. (C) Western blots of extracellular vesicles derived from intact- (Intact Exo) and apoptotic- (Apo Exo) m-cardiomyocytes. Positive control was from mouse kidney (Posi con). Samples corresponding to 5 μg protein were loaded in each lane. (D) Cardiac differentiation-related microRNAs in extracellular vesicles derived from intact- (Normal Exosome) and apoptotic- (Apoptotic Exosome) m-cardiomyocytes in qPCR (mean ± SE). *; $p<0.05$, **; $p<0.01$, ***; $p<0.001$. (E) Uptake of apoptotic-m-cardiomyocyte-derived extracellular vesicles into h-Muse cells. Extracellular vesicles (100 μg) prelabeled with green fluorescent PKH67 were added to $2x10^4$ h-Muse cells and incubated for 3 days. Bar = 25 μm.

SI 7) Macrophage marker expression in h-Muse cells and phagocytic activity of h-MSCs.

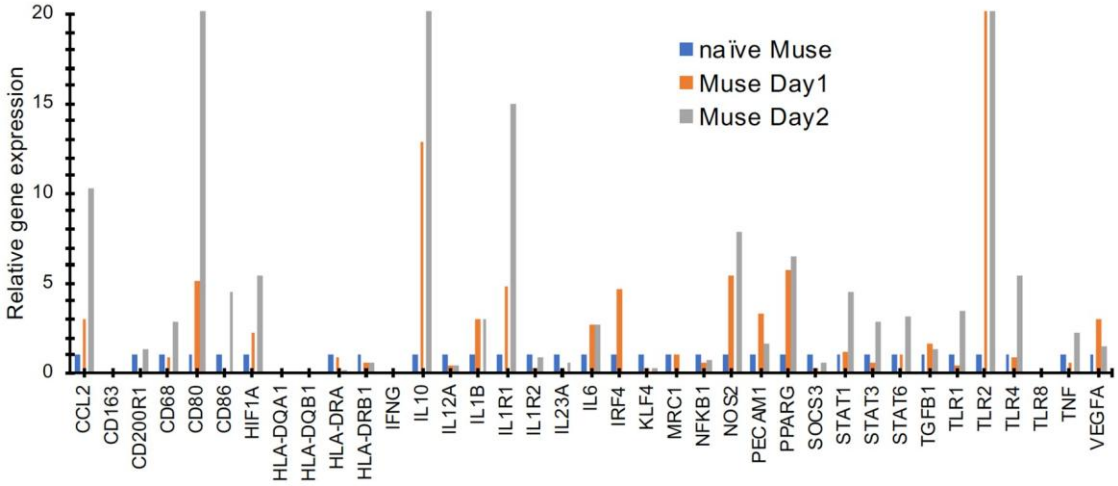

Figure S7. qPCR of macrophage markers in naïve h-Muse cells and h-Muse cells after 1 and 2 days exposure to m-cardiomyocyte-DDCs.

SI 8) Single-cell RNA sequencing of h-Muse cells after incubation with apoptotic cell fragments.

When cell cycle analysis was merged with t-SNE, the majority of naïve-Muse cell-cluster 2, as well as Phago-cardio-Muse, Phago-neuro-Muse 1~3, and Phago-hepa-Muse 1~4 were at G1 phase, whereas naïve 1 was in G2M and S phases (Fig. S8A). Thus, naïve 1 represented an actively proliferating population, whereas h-Muse cells became less proliferative after phagocytosing m-cardiomyocyte-, r-neural cell-, and r-hepatic cell-DDCs, showing that they began to differentiate into a specific lineage compatible with the cell type they had phagocytosed.

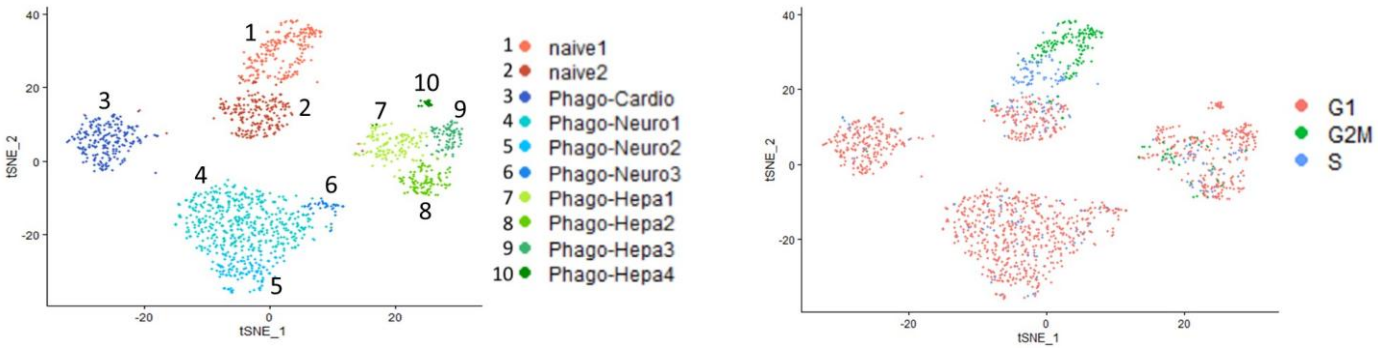

Figure S8A. Overlay of cell cycle analysis with t-SNE. t-SNE exhibited 2 clusters in naïve-Muse cells (naïve), 3 clusters in Phago-neuro-Muse, and 4 clusters in Phago-hepa-Muse, for a total 10 clusters including Phago-cardio-Muse, comprised of a single cluster (left, same as Figure 4B). These clusters are overlayed with the cell cycle analysis (right).

Because naïve-Muse cells were separated into subpopulations cluster1 and 2 by cell cycle as mentioned above, Phago-neuro-Muse and Phago-hepa-Muse groups that were separated into several clusters were further subjected to subpopulation analysis.

Phago-neuro-Muse was separated into the 3 clusters, namely Phago-neuro-Muse 1, -2, and -3. Glial-related markers, such as nuclear factor I X (*NFIX*) [4], semaphorin 3F (*SEMA3F*) [5], slit homolog 3 protein (*SLIT3*) [6], galactocerebrosidase (*GALC*) [7], junction adhesion molecule 3 (*LAM3*) [8], and NGFI-A-binding protein 2 (*NAB2*) [9], were mainly expressed in Phago-neuro-Muse 1/2 clusters; neuronal markers, such as B-cell translocation gene 2 (*BTG2*) [10], Ras GTPase SynGAP1 [11], bHLH family member e41 (*BHLHE41*) [12], and high-mobility group protein 2 (*HMG-B2*) [13], were mainly expressed in Phago-neuro-Muse 3 (Fig. S8B). Because r-neural cell-DDCs were generated from primary culture of rat fetal hippocampus, both apoptotic-glial and -neuronal cells were exposed to DDCs. Therefore, h-Muse cells that phagocytosed r-neural cell-DDCs, namely Phago-neuro-Muse, were considered to express both glial and neuronal markers.

Phago-hepa-Muse cells were separated into 4 clusters. Marker expression was analyzed with reference to the Human Protein Atlas [14]. Phago-hepa-Muse cluster-1 was characterized by a higher expression of endothelin 1 (*EDN1*), semaphorin 6B (*SEMA6B*), Kruppel-like factor 10 (*KLF10*), and integrin subunit alpha 1 (*ITGA1*), which are related to endothelial cells; Phago-hepa-Muse cluster-2 cells were characterized by the expression of Gardner-Rasheed feline sarcoma viral (*V-FGR*) oncogene homolog (*FGR*), guanylyl cyclase-coupled A (*GCA*), MX2, and C-X-C motif chemokine ligand 10 (*CXCL10*), which are related to Kupffer cells. On the other hand, Phago-hepa-Muse cluster-3/4 cells were higher in methyltransferase-like 7A (*METTL7A*), metallothionein 1M (*MT1M*), aldo-keto reductase family 1 member C2 (*AKR1C2*), nicotinamide N-methyltransferase (*NNMT*), Tsukushi, small leucine rich proteoglycan (*TSKU*), and aldehyde oxidase 1 (*AOX1*), which are related to hepatocytes. Similar to Phago-neuro-Muse, Phago-hepa-Muse cells were induced by phagocytosis of r-hepatic cell-DDCs prepared by the apoptotic treatment of primary cultured rat fetal liver. Because the primary culture of the liver contains liver components, hepatocytes, sinusoid endothelial cells, and Kupffer cells, h-Muse cells that phagocytosed r-hepatic cell-DDCs might have differentiated into these lineages.

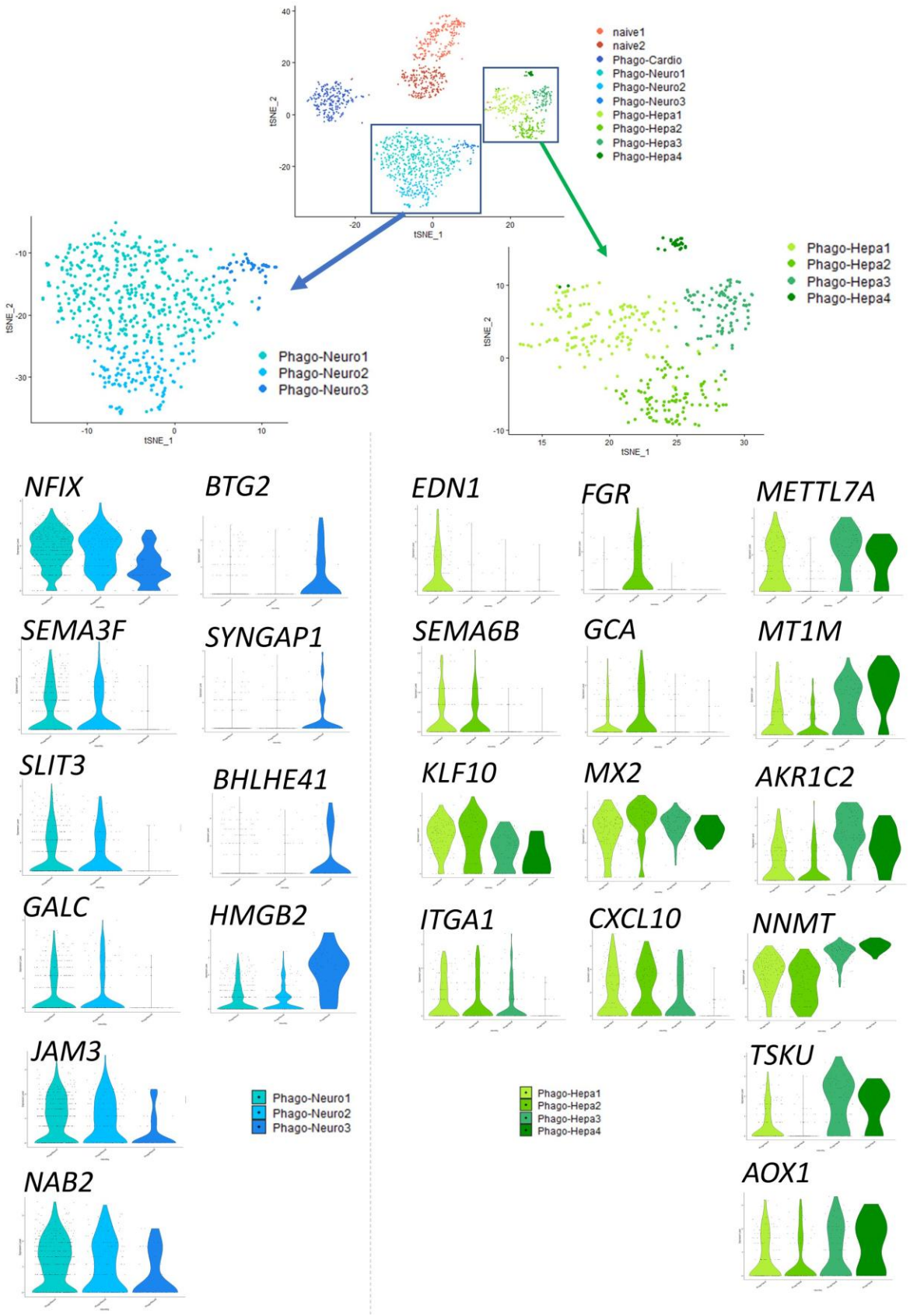

Figure S8B. Subpopulation analysis of Phago-neuro-Muse and Phago-hepa-Muse. Violin plots of each marker in each cluster are shown.

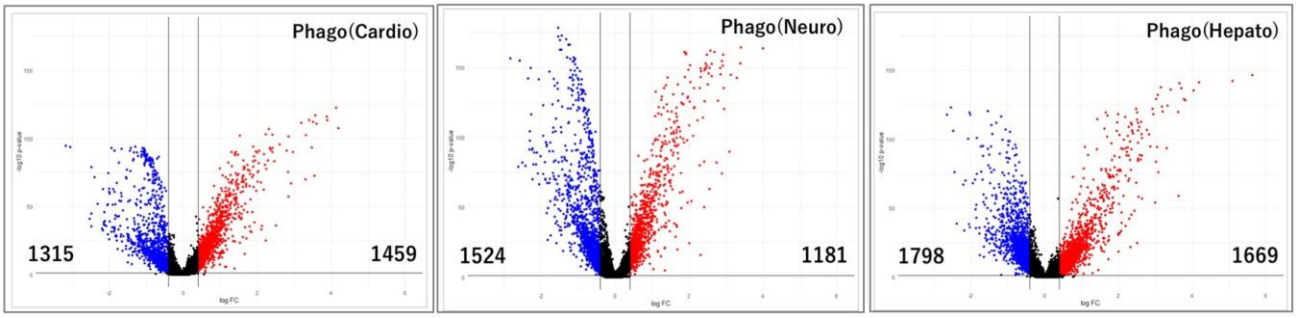

Figure. S8C. Volcano plot. Volcano plot of RNA-seq transcriptome data displaying the difference in the gene expression pattern between the naïve-h-Muse cells and each Phago-Muse group. Significantly differentially expressed genes were defined as those with a fold-change (FC) more than 1.5 times or less than 2/3 times, with $p<0.05$. Upregulated genes are shown in red, downregulated genes are shown in blue, and the black lines represent the boundary for identification of the upregulated or downregulated genes based on the p-value and FC. Genes that were increased (number of genes indicated on the right) and decreased (number of genes indicated on the left) were used for the GO analysis.

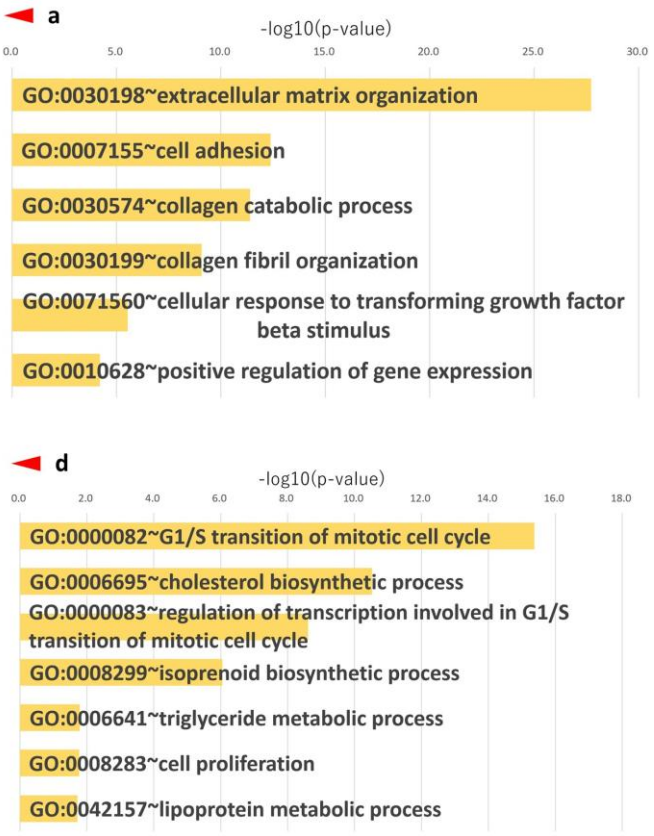

Figure S8D. GO term of arrowheads a and d in Fig. 5D.
Arrowhead a in Fig. 5D, common to naïve Muse cluster-1 and -2, included factors relevant to cell adhesion. Arrowhead d, common to Authen Cardio cluster-1 and -2, included factors relevant to cell cycle and lipid metabolism

SI 9) Effect of phagocytosis suppression on differentiation.

Effect of annexin V on h-Muse cell survival was evaluated (A). Effect of phagocytosis suppression by annexin V on the lineage-specific differentiation in h-MSCs (B) and r-NSCs (C). (B) Apoptotic m-adipocyte DDCs were treated with annexin V and incubated with h-MSCs. (C) Apoptotic h-neuronal cell DDCs were treated with annexin V and incubated with r-NSCs. (D-E) Western blot of each phagocytosis receptor in h-MSCs (D) and r-NSCs (E) in the naïve state and D2 after incubation with m-adipocyte- and h-neuronal cell-DDCs, respectively. Beta-actin (ACTB) is common to all the blots. The signal in the naïve cells is defined as 1. (F) CD36, ITGB3, CD91/LRP-1, and RAGE were each suppressed by small interference RNA (siRNA) in h-Muse cells, which were then exposed to m-cardiomyocyte DDCs. qPCR and Western blot confirmed the downregulated expression of each receptor type. On the basis of an on-target effect, significant decreases of both human-*NKX2.5* and -*GATA-4* ($p<0.05$) in CD36 and ITGB3, and significant decreases of either -*NKX2.5* or -*GATA-4* ($p<0.05$) in CD91/LRP-1 and RAGE were recognized at D7.

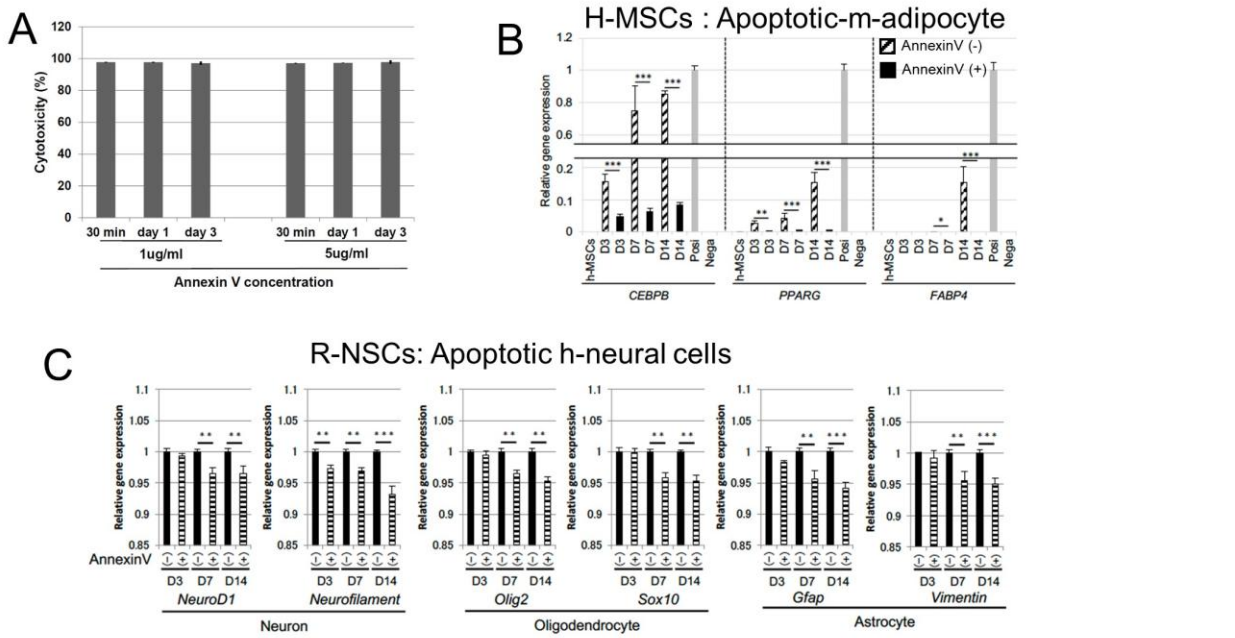
A
Cytotoxicity (%)
30 min
day 1
day 3
1ug/ml
5ug/ml
Annexin V concentration
B
H-MSCs : Apoptotic-m-adipocyte
AnnexinV (-)
AnnexinV (+)
Relative gene expression
h-MSCs
D3
D7
D14
Posi
Nega
CEBPB
PPARG
FABP4
C
R-NSCs: Apoptotic h-neural cells
Relative gene expression
AnnexinV
NeuroD1
Neurofilament
Olig2
Sox10
Gfap
Vimentin
Neuron
Oligodendrocyte
Astrocyte

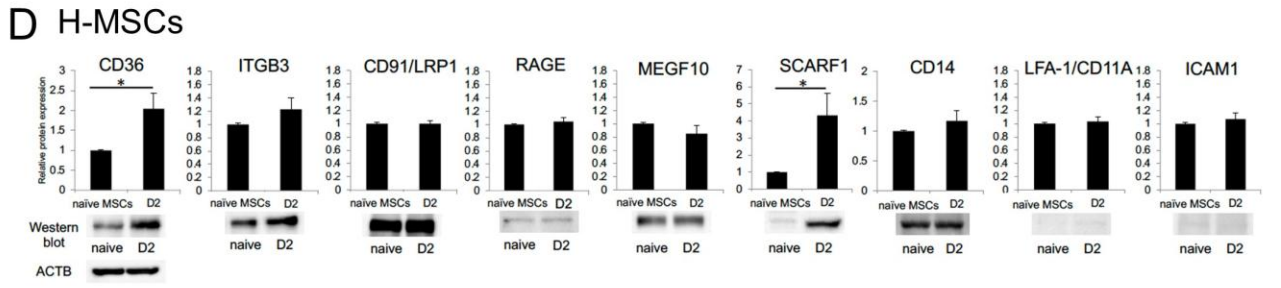
D H-MSCs
CD36
ITGB3
CD91/LRP1
RAGE
MEGF10
SCARF1
CD14
LFA-1/CD11A
ICAM1
Relative protein expression
naïve MSCs
D2
Western blot
naive
ACTB

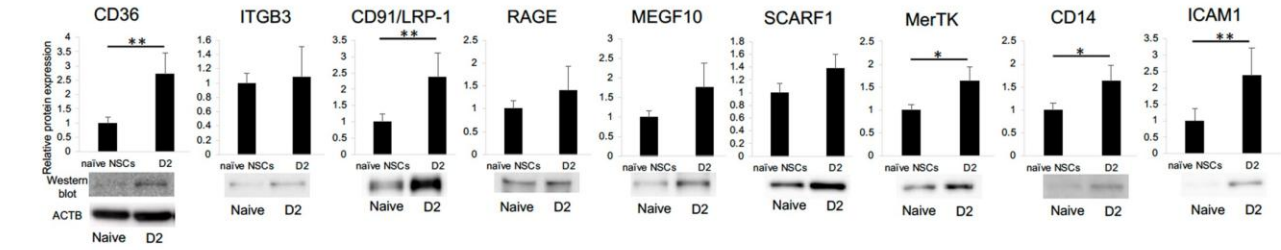
E R-NSCs
CD36
ITGB3
CD91/LRP-1
RAGE
MEGF10
SCARF1
MerTK
CD14
ICAM1
Relative protein expression
naïve NSCs
D2
Western blot
ACTB
Naive

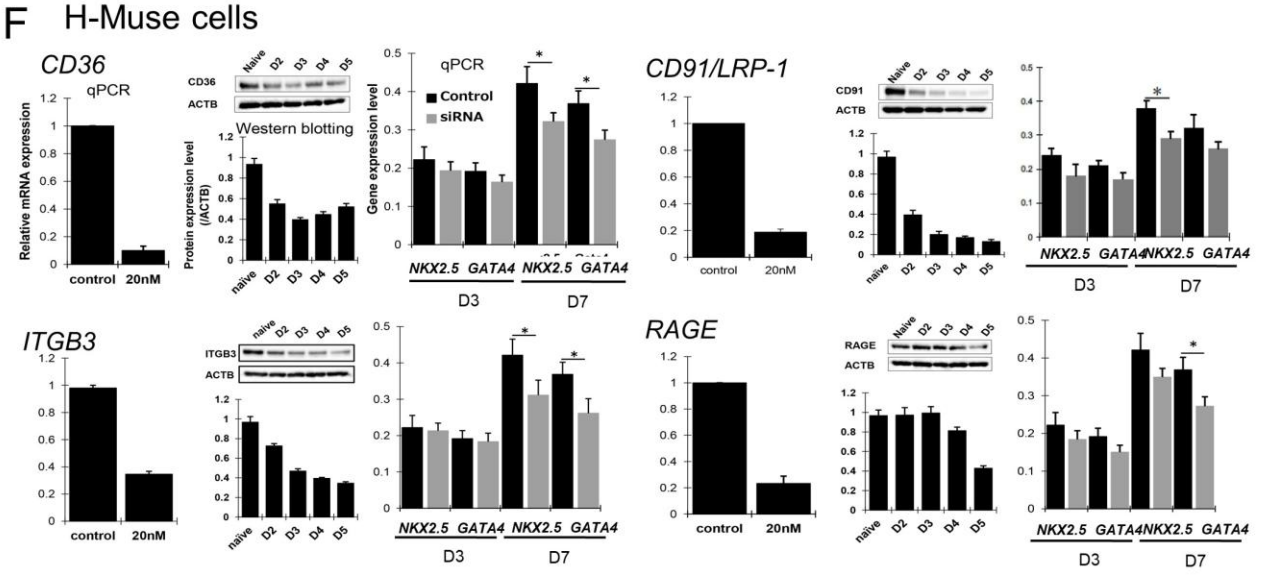
F H-Muse cells
CD36
qPCR
Relative mRNA expression
control
20nM
Western blotting
Protein expression level (/ACTB)
Gene expression level
Control
siRNA
NKX2.5
GATA4
D3
D7
CD91/LRP-1
ITGB3
RAGE

Fig. S9. Effect of phagocytosis suppression on differentiation. (A) The h-Muse cells were incubated in the presence of either 1 μg/ml or 5 μg/ml annexin V and the resulting cytotoxicity was measured at 30 min, 1 day, or 3 days using a Cytotoxicity LDH Assay Kit (Dojin Chemical, Japan). Annexin V did not induce cytotoxicity at any time-point at either concentration (mean ± SE). (B-C) Effect of phagocytosis suppression by annexin V and lineage-specific differentiation in h-MSCs (B) and r-NSCs (C). (D-E) Western blot of each phagocytosis receptor in h-MSCs (D) and r-NSCs (E). Beta-actin (ACTB) is common to all the blots. The signal in the naïve is set as 1. (F) siRNA for each phagocytosis receptor was introduced into h-Muse cells and then incubated with m-cardiomyocyte-DDCs. qPCR and Western blot confirmed the downregulated expression of each receptor type. The reduced expression of receptors was confirmed by qPCR and Western blot. Human-cardiac markers were examined by qPCR (mean ± SEM). *: p<0.05, **:p<0.01, ***:p<0.001.

SI 10) Effect of annexin V on phagocytosis activity of h-Muse cells.

(A) M-HL-1 cells expressing GATA-4-mCherry fusion protein (GATA-4-m-HL-1) was confirmed. (B-E) After annexin V treatment, DDCs derived from GATA-4-m-HL-1 were not successfully phagocytosed by h-Muse cells.

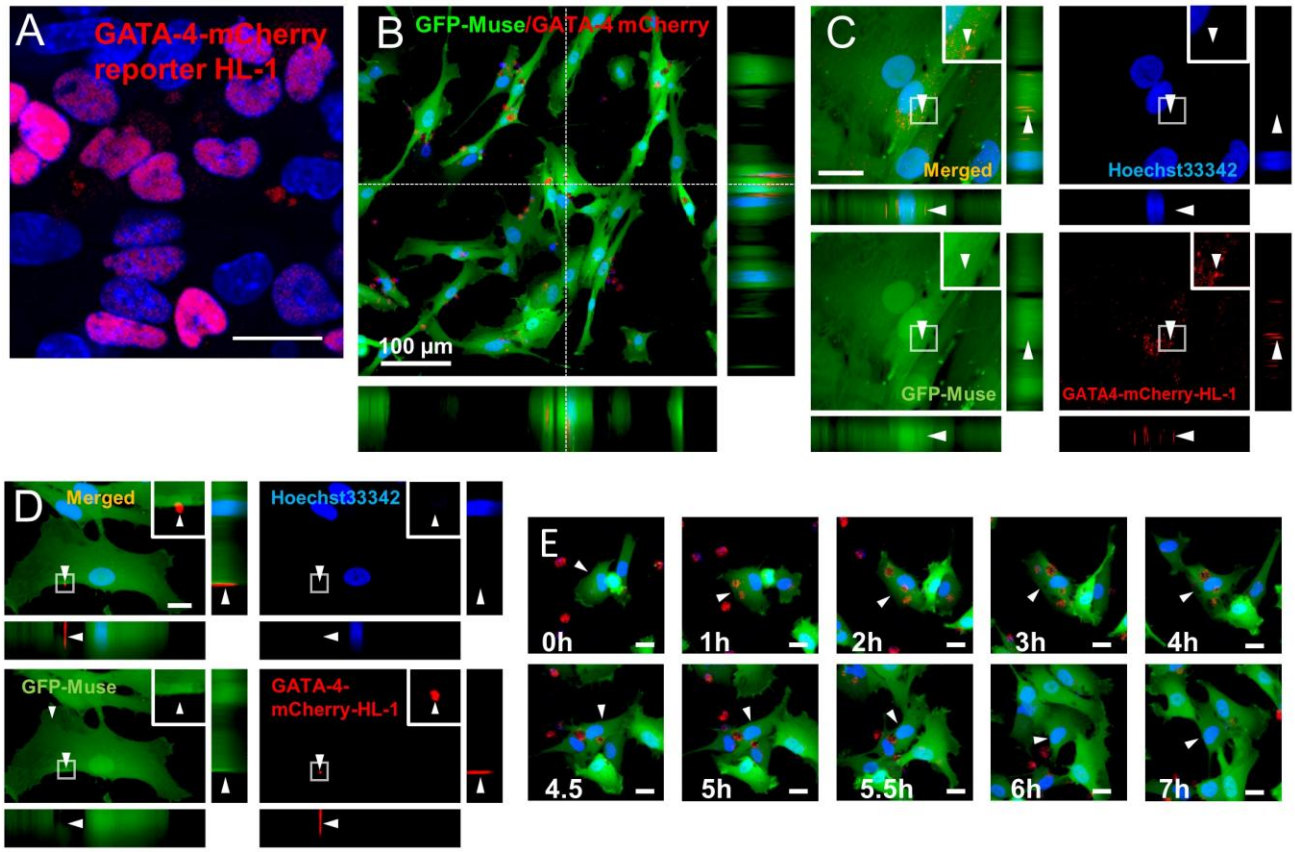

Figure S10. Phagocytosis of annexin V-treated apoptotic GATA-4-m-HL-1 fragments.
(A) GATA-4-mCherry fusion protein expression in the nucleus of GATA-4-m-HL-1. (B-E) Laser confocal microscopy images of GFP-h- Muse cells incubated with apoptotic-GATA-4 -m-HL-1-DDCs. (B) 10 h after incubation. GATA-4-mCherry fusion protein was taken up in the GFP-h-Muse cell cytoplasm. (C) 9 h after incubation. Phagocytosed GATA-4-mCherry fusion protein located in the GFP-h-Muse cell cytoplasm. (D) Incubation of GFP-h-Muse cells and annexin V-treated apoptotic-GATA-4-m-HL-1-DDCs at 24 h. The GATA4-mCherry signal was not incorporated into the GFP-h-Muse cell cytoplasm but was incorporated on the cell surface. (E) Incubation with annexin V-treated apoptotic GATA-4m-HL-1-DDCs. GATA-4-mCherry was at once phagocytosed and released to the extracellular space. Bars; A, C, D, E = 50 μm, B = 100 μm.

SI 11) Putative mechanism of how phagocytosis of differentiated cells regulates lineage-specific differentiation into the differentiated cell type.

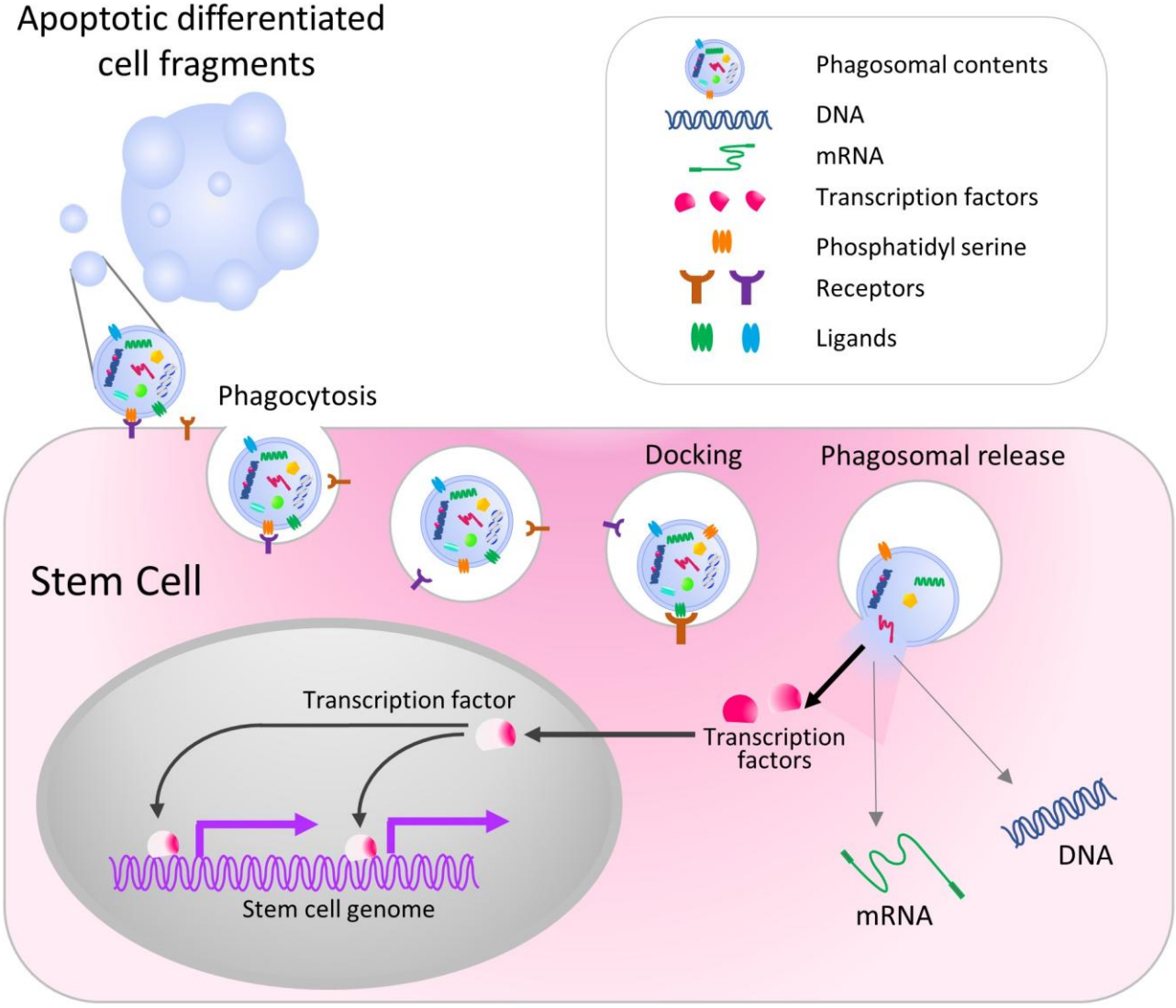

Figure S11. Schematic diagram of phagocytosis and lineage-specific differentiation.
Putative mechanism of how phagocytosis regulates commitment of stem cells (for example, Muse cells) to the phagocytosed cell lineage. DDC-derived transcription factors, proteins, DNA, and mRNA are released into the cytoplasm. Apoptotic cell-derived transcription factors might translocate to the nucleus and function directly in the stem cell.

SI 12) Phagocytotic activity of iPS cells.

Human fibroblast-derived iPS cells [15] labeled with PKH67 were incubated with apoptotic mCherry-m-Hepa1 DDCs. The phagocytosis rate was 4.9±1.5% at 5 h and 5.3±0.9% at 24 h, respectively.

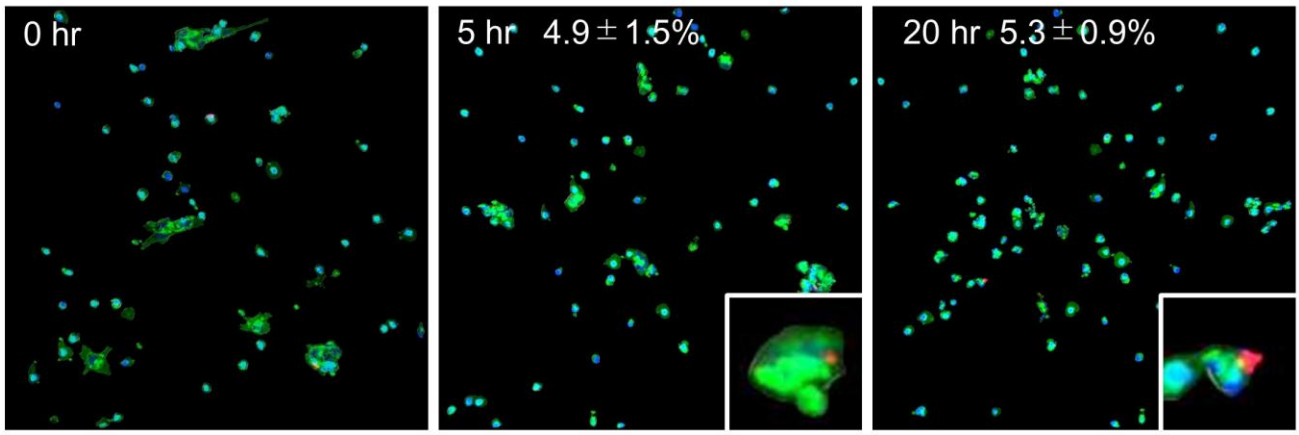

Figure S12. Images of h-iPS cells incubated with apoptotic mCherry-m-Hepa1 DDCs.

References

[1] M. Amin, Y. Kushida, S. Wakao, M. Kitada, K. Tatsumi, M. Dezawa, *Cell Transplantation* **2018**, *27* (2), 285, https://doi.org/10.1177/0963689717721514.

[2] A. Raso, E. Dirkx, *Noncoding RNA Res* **2017**, *2* (1), 27, https://doi.org/10.1016/j.ncrna.2017.03.001.

[3] a) J. S. Choi, H. I. Yoon, K. S. Lee, Y. C. Choi, S. H. Yang, I. S. Kim, Y. W. Cho, *J Control Release* **2016**, *222*, 107, https://doi.org/10.1016/j.jconrel.2015.12.018; b) Q. Xu, Y. Cui, J. Luan, X. Zhou, H. Li, J. Han, *Biochem Biophys Res Commun* **2018**, *498* (1), 32, https://doi.org/10.1016/j.bbrc.2018.02.144.

[4] E. Matuzelski, J. Bunt, D. Harkins, J. W. C. Lim, R. M. Gronostajski, L. J. Richards, L. Harris, M. Piper, *Dev Biol* **2017**, *432* (2), 286, https://doi.org/10.1016/j.ydbio.2017.10.019.

[5] S. A. Russell, G. J. Bashaw, *Dev Dyn* **2018**, *247* (4), 571, https://doi.org/10.1002/dvdy.24609.

[6] P. Palmquist-Gomes, J. A. Guadix, J. M. Perez-Pomares, *Dev Dyn* **2018**, *247* (5), 686, https://doi.org/10.1002/dvdy.24610.

[7] Y. Kondo, I. D. Duncan, *J Neurosci Res* **2016**, *94* (11), 1195, https://doi.org/10.1002/jnr.23909.

[8] O. Jahn, S. Tenzer, H. B. Werner, *Mol Neurobiol* **2009**, *40* (1), 55, https://doi.org/10.1007/s12035-009-8071-2.

[9] G. M. Mager, R. M. Ward, R. Srinivasan, S. W. Jang, L. Wrabetz, J. Svaren, *J Biol Chem* **2008**, *283* (26), 18187, https://doi.org/10.1074/jbc.M803330200.

[10] P. Iacopetti, G. Barsacchi, F. Tirone, L. Maffei, F. Cremisi, *Mech Dev* **1994**, *47* (2), 127, https://doi.org/10.1016/0925-4773(94)90085-x.

[11] J. S. Oh, P. Manzerra, M. B. Kennedy, *J Biol Chem* **2004**, *279* (17), 17980, https://doi.org/10.1074/jbc.M314109200.

[12] Y. Sun, H. Zhang, L. Wang, J. Li, H. Jin, Z. Wang, S. Tian, L. Qi, X. Liu, *Mol Cell Biochem* **2019**, *450* (1-2), 167, https://doi.org/10.1007/s11010-018-3383-z.

[13] A. Kimura, T. Matsuda, A. Sakai, N. Murao, K. Nakashima, *Dev Dyn* **2018**, *247* (1), 229, https://doi.org/10.1002/dvdy.24559.

[14] M. Uhlen, L. Fagerberg, B. M. Hallstrom, C. Lindskog, P. Oksvold, A. Mardinoglu, A. Sivertsson, C. Kampf, E. Sjostedt, A. Asplund, I. Olsson, K. Edlund, E. Lundberg, S. Navani, C. A. Szigyarto, J. Odeberg, D. Djureinovic, J. O. Takanen, S. Hober, T. Alm, P. H. Edqvist, H. Berling, H. Tegel, J. Mulder, J. Rockberg, P. Nilsson, J. M. Schwenk, M. Hamsten, K. von Feilitzen, M. Forsberg, L. Persson, F. Johansson, M. Zwahlen, G. von Heijne, J. Nielsen, F. Ponten, *Science* **2015**, *347* (6220), 1260419, https://doi.org/10.1126/science.1260419.

[15] S. Wakao, M. Kitada, Y. Kuroda, T. Shigemoto, D. Matsuse, H. Akashi, Y. Tanimura, K. Tsuchiyama, T. Kikuchi, M. Goda, T. Nakahata, Y. Fujiyoshi, M. Dezawa, *Proc Natl Acad Sci U S A* **2011**, *108* (24), 9875, https://doi.org/10.1073/pnas.1100816108.